Electronic Crystallization in a Lithium Battery Material: Columnar Ordering of Electrons and Holes in the Spinel $LiMn_2O_4$

J. Rodríguez-Carvajal,[1] G. Rousse,[2] C. Masquelier,[2] and M. Hervieu[3]
[1]*Laboratoire Léon Brillouin (CEA-CNRS), CEA/Saclay, 91191 Gif sur Yvette Cedex, France*
[2]*Laboratoire de Chimie des Solides, Université Paris-Sud, 91405 Orsay Cedex, France*
[3]*CRISMAT, ISMRA, 6 Boulevard du Maréchal Juin, 14050 Caen Cedex, France*
(Received 13 July 1998)

$LiMn_2O_4$ presents a first order structural transition at 290 K that was known to perturb the functioning as cathode in rechargeable Li batteries. We have solved the structure at 230 K and deciphered unambiguously the nature of this phase transition. The analysis of valence bond sums shows that the transition results from a partial charge ordering: two of the five Mn sites correspond to well-defined Mn^{4+} and the other three sites are close to Mn^{3+} ions. Charge ordering is accompanied by simultaneous orbital ordering due to the Jahn-Teller effect in Mn^{3+} ions. The microscopic details obtained from the structure are crucial for understanding the electron hopping persisting below the transition. [S0031-9007(98)07667-4]

PACS numbers: 61.50.Ks, 61.12.Ld, 61.14.–x, 71.38.+i

An increasing interest has developed around Li-Mn-O spinels due to their potential use as positive electrode materials in lithium rechargeable batteries. A vast majority of the studies devoted to these compounds deal with their electrochemical characteristics in lithium cells [1–3], but, only very recently, their structural and physical properties have also been studied [4–12]. The stoichiometric compound $LiMn_2O_4$ presents a first order structural transition [7–11] close to room temperature (RT) that was attributed to a Jahn-Teller distortion. On the other hand, in the last few years there has been an increasing interest in the electronic properties of oxides [13]. High temperature superconductivity and colossal magnetoresistance are well known examples in this field. In the case of Mn perovskites close to the composition $(R_{1/2}D_{1/2})MnO_3$ (R: trivalent rare earth; D: divalent ion), structural phase transitions accompanied by sharp modifications of electronic and magnetic properties have been attributed to charge ordering [14]. This phenomenon is supposed to be due to the Coulomb interaction that overcomes the kinetic energy of carriers below a certain temperature (Wigner crystallization) producing an alternating Mn^{3+}-Mn^{4+} NaCl-like lattice. This mechanism was first invoked by Verwey in 1941 to explain the low temperature transition in magnetite Fe_3O_4 as a Fe^{2+}–Fe^{3+} ordering within the B sites of the spinel structure [15]. The charge-ordering processes (sometimes called Verwey transitions) are fascinating phenomena that occur in systems with different crystal structures and give rise to different ordering patterns [16,17]. In spite of a different lattice organization of Mn ions in the spinel as compared to Mn perovskites, it is reasonable to expect some kind of similar electronic behaviors in both families. Most of the differences might possibly be explained by the different topology of the Mn-O sublattices.

To date, the structural details of charge-ordered Mn perovskites are quite limited since the superstructure reflections in neutron powder diffraction patterns are barely visible and single crystals show complicated twinning effects. This is also applicable to the structure of magnetite where the true crystal structure is yet not well established [18,19]. Electron diffraction provides the unit cell of the charge-ordered state, but only semiquantitative information can be obtained from the direct images [19].

It is extremely important to know whether the ionic picture usually invoked to describe the charge ordering in these materials is supported by structural experimental evidence. For instance, the simple NaCl-like ordering picture of Mn^{3+} and Mn^{4+} ions in $La_{1/2}Ca_{1/2}MnO_3$ has not yet been confirmed definitively even if experimental data are not in contradiction with such a picture. The need to constrain the structural parameters to successfully analyze the diffraction data [20] shows that the above-mentioned evidence is still lacking in the case of Mn perovskites. Here we show that the ionic picture is well supported in the case of $LiMn_2O_4$ spinel and we demonstrate that the charge-ordered state is not complete at 230 K.

Pure $LiMn_2O_4$ was prepared by two successive solid-state reactions of 8 h at 1073 K starting from Li_2CO_3 and MnO_2 [21]. Chemical titration of the sample provided an average valence for Mn of 3.50 ± 0.02. Differential scanning calorimetric experiments confirm the presence of a first order transition around RT. With a cooling rate of 5 K/min, the transformation cubic $\rightarrow$ orthorhombic starts at 290 K with a hysteresis of 10 K.

Neutron diffraction experiments were performed at the Orphée reactor at the Laboratoire Léon Brillouin. The high-resolution neutron powder diffractometer 3T2 was used for data collection with high direct space resolution ($\lambda = 1.225$ Å, $Q_{\max} = 9.2$ Å^{-1}) above and below the phase transition. A cryofurnace (sample under helium) was used to vary the temperature. Here we present the data collected at 230 and at 350 K. The program FULLPROF [22] was used for crystal structure refinement using the Rietveld method.

 0031-9007/98/81(21)/4660(4)$15.00

The high temperature form was carefully studied at 350 K [$a = 8.2495(2)$ Å] to confirm the crystalline quality and the stoichiometry of the sample. The refined structural parameters were (i) the oxygen parameter x of the Wyckoff site *32e* (space group $Fd3m$, origin choice at inversion center), (ii) the occupation of the oxygen site, (iii) the isotropic temperature factor of Li, and (iv) the anisotropic temperature factors of Mn and O. The final Bragg R factor was 1.2%. The refined value of x was 0.26301(3) and the oxygen occupation refined to the nominal value within the experimental error. The unique Mn-O distance is 1.9609(3) Å, which is intermediate between what is expected for Mn^{3+}-O and Mn^{4+}-O bond lengths. A valence bond analysis [23–25] assuming Mn^{3+}-O^{2-} gives an effective valence of 3.45 valence units (v.u.). Using the Mn^{4+}-O^{2-} d_0 parameter [23], the valence obtained is 3.39 v.u. The correction of the calculated valence for using d_0 for RT is negligible ($\Delta V < 0.02$ v.u.) [25].

The neutron powder diffraction patterns at low temperature showed many small superstructure reflections, which we recognized immediately to be at the origin of a big unit cell. The indexing of the pattern using solely the neutron data was ambiguous and gave several reasonable solutions due to the strong overlap between neighboring reflections. The information provided by electron diffraction at different temperatures was of capital importance for finding the $Fddd$ "$3a \times 3a \times a$" cell. Similar observations were recently reported by Oikawa *et al.* [10] who propose an average orthorhombic structure [$a = 8.2797(2)$, $b = 8.2444(3), c = 8.1981(2)$ Å] to describe their neutron diffraction pattern, despite evidence of a tripled periodicity in their electron diffraction photographs.

The sample for electron microscopy was prepared by crushing the crystals in alcohol. The small flakes in suspension were deposited on a holed carbon film, supported by a copper grid. The electron diffraction (ED) study versus temperature was carried out with a JEOL 2010 electron microscope fitted with a double tilt cooling sample holder (±40°). The ED patterns were recorded from 92 K to RT keeping a constant electron current density. At the lowest temperature we studied the ED patterns of thirty crystals. All of them can be indexed considering a spinel-type subcell with a system of extra reflections. A large majority of the crystallites (26/30) exhibit a common $3a \times 3a \times a$ supercell, whereas the others (4/30) are characterized by a different superstructure that transformed to the $3a \times 3a \times a$ supercell on heating. The reconstruction of the reciprocal space was carried out, for the majority phase, by tilting around the main crystallographic axes. The extinction conditions are compatible with the $Fddd$ space group. The same reciprocal plane ([001] zone axis, $hk0$ reflections) is shown for the high temperature phase [Fig. 1(a)] and for the low temperature phase [Fig. 1(b)].

The structure of the low temperature form was solved with the help of a program that generates atoms in supercells with changes of origin. The final atom positions are given in Table I. It is worth mentioning that five sites of

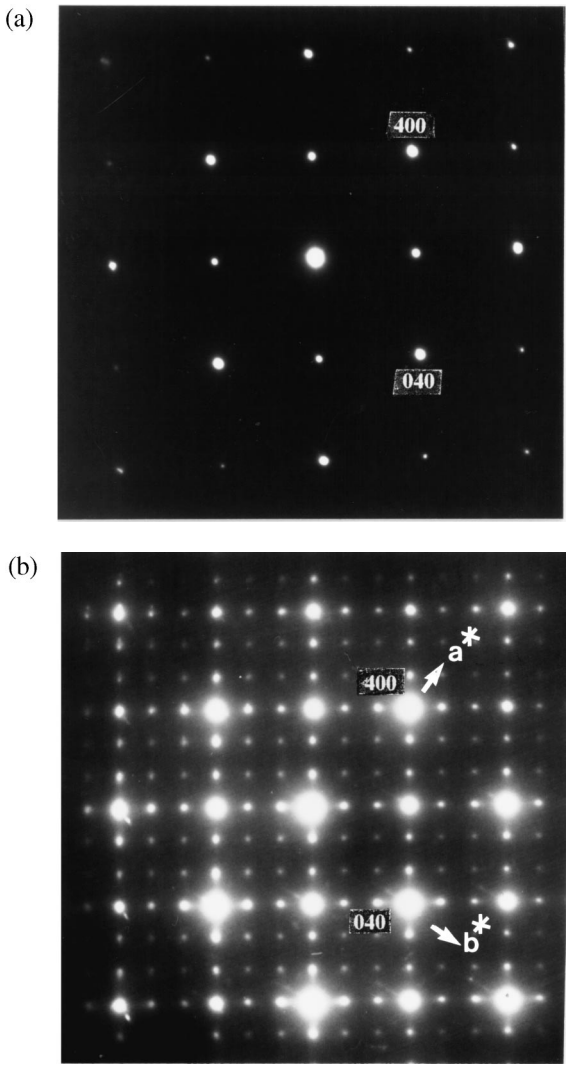

FIG. 1. Electron diffraction patterns along [001] of the high (a) and low (b) temperature phases of stoichiometric $LiMn_2O_4$. Indices are referred to the cubic $Fd3m$ spinel lattice.

Mn ions are found so that the crystal structure does not support a total charge ordering that needs an even number of sites for the $Mn^{3+}/Mn^{4+} = 1$ ratio. In Fig. 2 parts of the observed and calculated diffraction patterns are shown for both phases.

Electronic conductivity measurements [21] gave similar results to those already published [9], showing an abrupt increase of resistivity upon cooling to the low temperature phase. The activation energy of the low temperature form is slightly higher but similar to that of the high temperature. This fact was interpreted [8–10] as the consequence of the appearance of a new insulating "tetragonal phase" coexisting with a smaller volume fraction of cubic phase. Our study reveals that only one phase, orthorhombic, exists at 230 K. The charge carriers are very probably Jahn-Teller small polarons.

The analysis of the structure obtained from the Rietveld refinement of our neutron data clearly shows the electron ordering nature of the phase transition and allows us to

TABLE I. Structural parameters of the low temperature phase of $LiMn_2O_4$ at 230 K. The space group is $Fddd$. Isotropic temperature factors have been constrained to be the same for each element. The average M-O distances (M = Mn, Li) are in Å. The valence bond sum (VBS) is calculated using the Zachariasen formula: $V_i = \sum_j s_{ij} = \sum_j \exp[(d_0 - d_{ij})/0.37]$ using the parameters d_0, characterizing a cation-anion pair, from Ref. [23]. The final calculations for Mn ions have been performed assuming a d_0 of Mn^{3+}-O^{2-} for Mn(1), Mn(2), and Mn(3) and a d_0 of Mn^{4+}-O^{2-} for Mn(4) and Mn(5). The distortion parameter Δ of a coordination polyhedron BO_N with an average B-O distance $\langle d \rangle$ is defined as $\Delta = (1/N)\sum_n [(d_n - \langle d \rangle)/\langle d \rangle]^2$. Cell parameters: $a = 24.7435(5)$, $b = 24.8402(5)$, $c = 8.1989(1)$ Å. Total number of reflections: 2014. Total number of structural parameters: 47. Conventional Rietveld R factors: $R_P = 5.87\%$, $R_{WP} = 5.92\%$, $R_{exp} = 3.97\%$, $\chi^2 = 2.22$. Bragg R factor: 2.03%.

Atom	x	y	z	Biso (Å^2)	Wyckoff site	d(Mn-O) (Å)	Valence sum	Distortion ($\times 10^{-4}$)
Mn(1)	$\frac{1}{4}$	$\frac{1}{4}$	$\frac{1}{2}$	0.28(2)	16d	2.003(2)	3.20(2)	20.6
Mn(2)	0.0803(3)	0.0855(3)	0.5035(9)	0.28(2)	32h	1.995(4)	3.27(3)	19.4
Mn(3)	0.0839(4)	0.3301(3)	0.2480(16)	0.28(2)	32h	2.021(5)	3.12(5)	36.6
Mn(4)	0.2527(3)	0.1675(3)	0.2491(13)	0.28(2)	32h	1.903(4)	4.02(5)	4.6
Mn(5)	0.1648(3)	0.2447(2)	0.2429(11)	0.28(2)	32h	1.916(4)	3.90(4)	6.1
Li(1)	$\frac{1}{8}$	$\frac{1}{8}$	$\frac{1}{8}$	0.77(6)	8a	1.967(2)	1.033(6)	0
Li(2)	$\frac{3}{8}$	0.2116(10)	$\frac{3}{8}$	0.77(6)	16f	1.984(8)	0.99(2)	0.5
Li(3)	0.2054(11)	$\frac{3}{8}$	$\frac{3}{8}$	0.77(6)	16e	2.016(8)	0.91(2)	0.3
Li(4)	0.2919(8)	0.2953(9)	0.1191(16)	0.77(6)	32h	1.946(9)	1.10(3)	7.5
O(1)	0.1754(2)	0.1682(2)	0.2565(5)	0.522(6)	32h	···	2.02(2)	···
O(2)	0.0786(2)	0.0070(2)	0.4805(8)	0.522(6)	32h	···	1.98(3)	···
O(3)	0.0783(2)	0.3311(2)	0.4795(9)	0.522(6)	32h	···	1.94(3)	···
O(4)	0.2528(2)	0.1732(2)	0.4747(8)	0.522(6)	32h	···	2.06(3)	···
O(5)	0.0055(2)	0.0080(2)	0.2419(6)	0.522(6)	32h	···	1.88(3)	···
O(6)	0.2559(2)	0.0887(2)	0.2375(9)	0.522(6)	32h	···	2.05(3)	···
O(7)	0.1621(2)	0.3225(2)	0.2382(9)	0.522(6)	32h	···	2.04(3)	···
O(8)	0.0908(2)	0.2434(2)	0.2354(8)	0.522(6)	32h	···	2.17(3)	···
O(9)	0.0843(2)	0.1610(2)	0.5150(6)	0.522(6)	32h	···	2.07(3)	···

interpret the resistivity measurements. The data presented in Table I correspond to a structure refinement performed at 230 K. The use of the RT values for d_0 in Table I does not change our conclusions because the correction is negligible ($\Delta V < 0.02$ v.u.). Two Mn sites [Mn(4), Mn(5)] correspond to well-defined Mn^{4+} ions (the average Mn-O distance is 1.91 Å). The interpretation of this result is that these sites appear to be forbidden for electron hopping. The other three sites [Mn(1), Mn(2), and Mn(3)] are not pure Mn^{3+} ions. This is revealed by the average Mn-O distance for the three Mn sites (2.00 Å), which is slightly smaller than what is expected for pure Mn^{3+} (2.02 Å). To simplify the visualization of the crystal structure, we have represented in Fig. 3 an idealized projection along [001] of the Mn and Li sites within a unit cell. Oxygen atoms have been removed from the drawing. We have used the same symbol to represent all the Mn^{3+}-like sites and another symbol for the two Mn^{4+} sites. Neglecting the z position of the atoms, it is apparent that octagonal cylinder surfaces (hole-rich regions), containing all the Mn^{4+}, wrap two types of Mn^{3+} columns (electron-rich regions) which are distinguished by the presence, or lack thereof, of Li ions. The space between the octagonal cylinders is occupied by columns containing the Mn(1) site in the special position (16d).

The average valence of Mn ions, obtained from chemical analysis and structure refinement at high temperature, indicates that the number of holes (Mn^{4+}) in the e_g band is equal to the number of electrons (Mn^{3+}) available for hopping. The crystal structure indicates that there are 64 [32 Mn(4) + 32 Mn(5)] localized holes per unit cell, so there are eight remaining holes per cell distributed within the 80 [16 Mn(1) + 32 Mn(2) + 32 Mn(3)] Mn positions. Thus, a certain electron hopping should persist at low temperature as revealed by the previous analysis. This is perfectly consistent with the semiconducting characteristics of the compound below the transition temperature and explains the weak change in the activation energy through the transition. The diminution of the conductivity upon cooling is primarily due to the diminution of the number of carriers and of the number of sites available for hopping. The static distortion of the three $Mn^{3+}O_6$ octahedra (Table I) is consistent with a slightly attenuated Jahn-Teller effect [26] due to the remaining electron hopping towards the eight holes per cell. The charge ordering process is, consequently, accompanied by the presence of an orbital ordering which is the manifestation of the Jahn-Teller polaronic nature of the mobile charges above and below the transition temperature.

To our knowledge this is the first time that a partial charge-ordering transition is clearly observed in a Mn oxide. The transition to a totally charge-ordered state at lower temperature should not be disregarded. The observation in ED patterns of some crystallites with a more

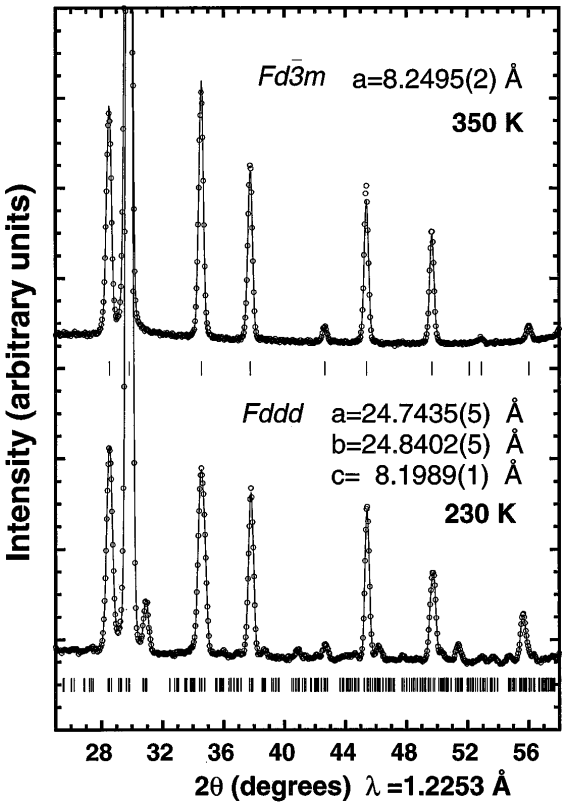

FIG. 2. Details of the observed and calculated neutron diffraction patterns ($\lambda = 1.2253$ Å) of the high temperature charge-disordered phase (350 K), and of the low temperature partially charge-ordered phase (230 K) of $LiMn_2O_4$. Additional tick marks in the low temperature pattern correspond to the superstructure reflections.

complex superstructure at 92 K may indicate the onset of such a phase transition. The electronic crystallization observed in this compound must be due to a combination of Coulomb interaction and another mechanism implying electron-lattice coupling as in the Jahn-Teller effect. The observed charge-ordering pattern at 230 K cannot be the ground state of the electronic system in $LiMn_2O_4$. If we consider just screened Coulomb interaction, alternating Mn^{3+}-Mn^{4+} patterns are favored. The study of the magnetically ordered ground state is under way.

The authors gratefully acknowledge Dr. Mitsuharu Tabuchi (ONRI, Japan), Professor Ryoji Kanno (Kobe University), and Y. Matsui (NIRIM, Japan) for fruitful discussions. One of us (G. R.) thanks Union Minière for financial support.

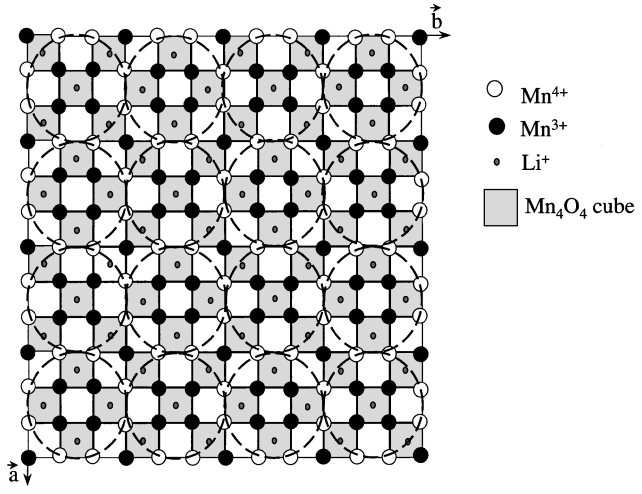

FIG. 3. Simplified projection of the charge partially ordered structure. Static holes (Mn^{4+}, open circles) wrap columns of nearly pure Mn^{3+} ions along the c axis. $\frac{8}{72} = \frac{1}{9}$ of the total number of holes are mobile within the Mn^{3+} sublattices.

[1] M. M. Thackeray, Prog. Solid State Chem. **25**, 1 (1997), and references therein.
[2] R. J. Gummow, A. de Kock, and M. M. Thackeray, Solid State Ionics **69**, 59 (1994).
[3] D. Guyomard and J. M. Tarascon, Solid State Ionics **69**, 222 (1994).
[4] Y. Gao and J. R. Dahn, Solid State Ionics **84**, 33 (1996).
[5] C. Masquelier *et al.*, J. Solid State Chem. **123**, 255 (1996).
[6] V. Massarotti *et al.*, J. Solid State Chem. **131**, 94 (1997).
[7] A. Yamada and M. Tanaka, Mater. Res. Bull. **30**, 715 (1995).
[8] A. Yamada, J. Solid State Chem. **122**, 160 (1996).
[9] Y. Shimakawa, T. Numata, and J. Tabuchi, J. Solid State Chem. **131**, 138 (1997).
[10] K. Oikawa *et al.*, Solid State Ionics **109**, 35 (1998).
[11] H. Yamaguchi, A. Yamada, and H. Uwe, Phys. Rev. B **58**, 8 (1998).
[12] P. Strobel *et al.*, J. Solid State Chem. **135**, 132 (1998).
[13] N. Tsuda, K. Nasu, A. Yanase, and K. Siratori, *Electronic Conduction in Oxides* (Springer-Verlag, Berlin, 1991).
[14] Y. Tomioka *et al.*, Phys. Rev. Lett. **74**, 5108 (1995).
[15] E. J. W. Verwey and P. W. Haaymann, Physica (Utrecht) **8**, 979 (1941).
[16] Special issue on Verwey transition [Philos. Mag. B **42**, No. 3 (1980)].
[17] S. Mori, C. H. Chen, and S.-W. Cheong, Nature (London) **392**, 473 (1998).
[18] M. Iizumi *et al.*, Acta Crystallogr. Sect. B **38**, 2121 (1982).
[19] N. Otsuka and H. Sato, J. Solid State Chem. **61**, 212 (1986).
[20] P. Radaelli, D. E. Cox, M. Marezio, and S.-W. Cheong, Phys. Rev. B **55**, 3015 (1997).
[21] G. Rouse *et al.* (unpublished).
[22] J. Rodríguez-Carvajal, Physica (Amsterdam) **192B**, 55 (1993).
[23] I. D. Brown and D. Altermatt, Acta Crystallogr. Sect. B **41**, 244 (1985).
[24] I. D. Brown, Acta Crystallogr. Sect. B **48**, 553 (1992).
[25] I. D. Brown, A. Dabkowski, and A. McCleary, Acta Crystallogr. Sect. B **53**, 750 (1997).
[26] J. Rodriguez-Carvajal *et al.*, Phys. Rev. B **57**, R3189 (1998).